PCCP

Accepted Manuscript

ROYAL SOCIETY OF CHEMISTRY

www.rsc.org/pccp

Physical Chemistry Chemical Physics
CREATED USING THE RSC LaTeX PCCP ARTICLE TEMPLATE – SEE www.rsc.org/electronicfiles FOR DETAILS
ARTICLE TYPE
www. rsc.org/xxxxxx | XXXXXXXX

Band Gap Modulation of Functionalized Metal-Organic Frameworks

Terence Musho,[*a] **Jiangtan Li,**[a] **and Nianqiang Wu**[a]

Received Xth XXXXXXXXXX 20XX, Accepted Xth XXXXXXXXX 20XX
First published on the web Xth XXXXXXXXXX 200X
DOI: 10.1039/b000000x

Metal-organic framework (MOF) have been envisioned as an alternative to planar metallic catalysis for solar-to-fuel conversion. This is a direct result of their porous structure and the ability to tailor their optical absorption properties. This study investigates the band gap modulation of Zr-UiO-66 MOF from both a computational and experimental point of view for three linker designs that include benzedicarboxylate (BDC), BDC-NO_2, and BDC-NH_2. Emphasis in this study was aimed at understanding the influence of the bonding between the aromatic ring and functional group. A ground state density functional theory (DFT) calculation was implemented to investigate the projected density of states and the origins of the modulation. A time-dependent density functional theory (TDDFT) calculation of the hydrogen terminated linkers confirmed the modulation and accounted for the electron charge transfer providing comparable optical band gap predictions to experimental results. Computational results confirmed the hybridization of the carbon-nitrogen bond in conjunction with the donor state resulting from the NH_2 functionalization. The NO_2 functionalization resulted in an acceptor configuration with marginal modification to the valence band maximum. The largest modulation was BDC-NH_2 with a band gap of 2.75eV, followed by BDC-NO_2 with a band gap of 2.93eV and BDC with a band gap of 3.76eV. The electron effective mass was predicted from the band structure to be 8.9m_e for all MOF designs.

1 Introduction

Recent development of new materials for advanced gas adsorbents[1–5] with applications in both hydrogen fuel storage and hydrogen fuel conversion[6] have been of growing interest. These recent efforts have been aimed at developing and synthesizing not only highly selective[5] materials but also organic materials that are thermally stable[7] and electrically conductive[8]. In the application of these new materials for solar-to-fuel catalytic conversion of hydrogen, there are currently two major limitation that prevent traditional planar metallic solutions. Those first limitation is the availability of reaction centers, which is a function of surface area and the number of activated catalytic ions. The second limitation is a broad utilization of the visible region of the electromagnetic spectrum for carrier ionization. By tailoring the band gap of the photocatalyst material, more specifically, decreasing the band gap energy the second limitation can be addressed. Similarly, if a porous medium can be utilized the areal density of reaction sites can be significantly increased addressing the first issue. In providing a solution to both of these issues in a single material, the following study investigates a new type of metal-organic frameworks (MOFs) that embody both of these desirable material attributes.

Metal-organic frameworks have several advantageous attributes for photocatalysis. The most advantageous being their porous or open structure that results in increase surface area for increased throughput of reactions. The second aspect is the ability to modulate the band structure or optical absorption characteristics through a modification of the ligand coordination, what will be referred to as the linker in the follow study. These advantageous attributes come at a limitation of sensible operational temperature and stability of the MOF material. For this study the selection of the MOF structure has been limited to a zirconium based MOF that has been

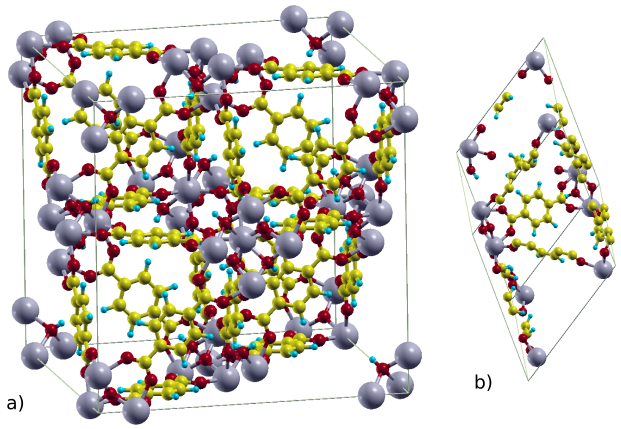

Fig. 1 An illustration of the unit cell of a Zr-UiO66-BDC. Part (a) is the 456 atom conventional unit cell and part (b) is the 114 atom primitive unit cell. A large pore can be visualized in the body-center of the conventional unit cell.

[a] *Department of Mechanical and Aerospace Engineering, West Virginia University, Morgantown, WV 26506-6106, USA. Fax: 304-293-6689; Tel: 304-293-3256; E-mail: tdmusho@mail.wvu.edu*

previously demonstrated to be stable up to 300-400°C. The following study will rely on a combination of first principle density functional theory (DFT) and time-dependent density functional theory (TDDFT) predictions that are verified and validated with experimental results. The specific MOF structure selected for this structure will be a Zr-UiO66-BDC-R, {R=H,NH2,NO2} MOF were the benzenedicarboxylate (BDC) is modified with an amine group, NH_2 and a nitro group NO_2.

In photochemical conversion applications the band gap is critical to providing a large enough over-potential to surpass the potential of the reaction barrier. While at the same time, not increasing the phonon production significantly such that there is a large increase in material temperature. Granted a significant phonon population will aid in the excitation of electrons through electron-phonon scattering process, however, subsequently the mobility of electrons is significantly diminished. The significant decrease in mobility is directly related to the conversion efficiency and is often a limitation of organic crystal semiconductors. A means of avoid this limitation is to decrease the optical band gap of the material. In doing so, two attributes are influenced, 1) a larger extend of the visible spectrum can be utilized, and 2) decreased operational temperatures.

Previously, researchers have demonstrated from both an experimental[9–12] and a computational point of view[13–15] that the linker coordination can be used as a mechanism to modulate the band gap of these MOF material. It is interesting to note that recent studies in the literature have suggested conflicting theories to the exact origins of the band gap modulation. Original research[15] of these MOFs suggested that the carbon atom in the aromatic ring are responsible for the modulation of the band gap. More recent research[14] suggests that the oxygen near the metalloid cluster is responsible for the modulation. Granted both of these studies do confirm the apparent modulation of the optical properties. The following study will clarify this discrepancy by investigating the origins of the modulation by using first principle computational models to analyze the projected density of state of the orbitals, which has not previously been investigated for these particular MOF designs. Additionally, this study will investigate the optical absorption of the linkers and the effective band gap from a time-dependent density functional theory point of view. Validation of the computational prediction will be obtained through the comparison to experimental results.

1.1 Material Design

The metal-organic structure of interest in this research has zirconium (Zr) incorporated metalloid at the corners and a single length linker (UiO-66). The unit cell description of a Zr-UiO-66 MOF is shown in Figure 1. Part a of Figure 1 is an illustration of the conventional unit cell with 456 atoms. At the body-centered position of the conventional unit cell is a void or pore. The dimensions of this pore can be increased by increasing the length of the linker. Part b of Figure 1 is the 114 atom primitive unit cell for the Zr-UiO-66 MOF. To alleviating the computational expense of the first principle calculations the primitive unit cell was used for this study.

In this study the linker was modified with two other functional groups. Those groups were NH_2 and NO_2. An illustration of the linkers taken from the optimized unit cell description are shown in Figure 2. Part a in the Figure 2 is the BDC hydrogen terminated linker, part b is the BDC-NH_2 attachment in place of one of the hydrogen atoms. Note the BDC-NH_2 linker is planar with the benzene plane. The third linker in part c is the BDC-NO_2 that replaces one of the hydrogen atoms. In the optimized structure for BDC-NO_2 there is a slight rotation out of the benzene plane that can be related to the bonding nature of this functional group.

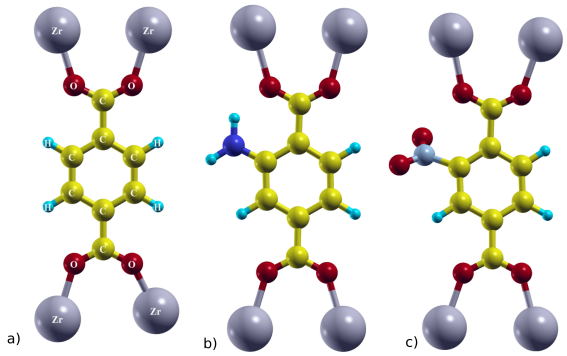

Fig. 2 An illustration of the unit cell of a three linker design. Part (a) is UiO-66-H, part (b) is UiO-66-NH_2, and part (c) is UiO-66-NO_2.

1.2 Computational Details

The density functional theory calculation were carried out using the Quantum Espresso package[16]. The ground state calculation were calculated on a Monkhorst-Pack 4x4x4 k-point grid with an half step offset of $\{1/4, 1/4, 1/4\}$ in the primitive unit cell. The density of state calculations were calculated with a k-point grid of 4x4x4 and no offset. All structures were relaxed to a stress less than 0.5kPa. A single super-cell size of 2x1x1 primitives was also calculated for the BDC design to confirm there were no discrepancies arising from neighboring unit cells not explicitly modeled in the single primitive calculations.

Several functionals were investigated that included BLYP, PBE, and their hybrid counterparts (B3LYP, PBE0), which include a fraction of the exact exchange. The BLYP functional had evidence of over binding of the carbon atoms distorting the internal pore structure towards a fullerene state. This distortion also proved to reduce the apparent band gap energy.

Comparing B3LYP to BLYP for the BDC linker there was a 0.6eV decrease in the p-orbital band gap for the B3LYP functional. In the case of BLYP to PBE there was increase in band gap of the p-orbitals of approximately 0.5eV for PBE. This favored the selection of PBE over BLYP. In the case of PBE0 compared to PBE there was no apparent change in band gap. The PBE functional proved to be most well behaved and has been successfully used in other studies [14]. Therefore, the PBE functional was selected for the entirety of this study.

All pseudopotentials were non-relativistic RRJK3 ultrasoft potentials. The carbon had a basis of 2s2 2p2. Hydrogen basis was 1s1. Nitrogen basis was 2s2 2p3. Oxygen basis was 2s2 2p4. Zirconium basis was 4s2 2p6 4d2 5s2 5p0. A kinetic energy cut-off of 50 Ry and a charge density cut-off of 200 Ry was used for all pseudopotentials. As highlighted in the previous paragraph, there was no significant improvement of the band gap when the exact exchange was added to the PBE functional. Granted the inclusion of exact-exchange is often necessary in molecular system to account for the non-locality of the hole in gradient approaches, such as the generalized gradient approach (GGA) [17]. However, the addition was not warranted in this study. This can be attributed to the fact that the system involves hydrides that are well treated with pure gradient approaches in the absence of exact exchange [18]. However, the PBE functional is still susceptible to over-binding of the hydrogen [19] and is responsible for underestimate of the band gap. The reader should be aware both density functional theory with and without exact exchange is not a ideal technique to describe absolute band gaps but provides a means for relative comparison of band gaps.

The time-dependent density functional perturbation theory (TDDFT) calculations were carried out in the similar manner with the same PBE functional. The only exception was a subset of the MOF structure was simulated to alleviate the computational expense. The subset model included only the hydrogen terminated linkers in an isolated box. In modeling the isolated linker, it is assumed that strong interaction between neighboring linkers is negligible. The distance to the closest neighboring distance is approximately 5.8Å. This is approximately four times larger than a C-C bond. The assumption of negligible long range interaction is also imposed when isolating the linker. In addition to neglecting the neighboring interaction, it is assumed that the metalloid at the corner of the MOF does not influence the optical absorption. This is assumed reasonable as the Zr atom has metallic bonding and d-orbital interaction with oxygen. Thus having no influence on the p-orbital of the benzene and the functional group, which is responsible for the optical absorption. This cluster modeling approach of only the hydrogen terminated linkers has been applied successfully in the literature [20,21]. In addition to modeling only the linker, the k-point grid for the TDDFT were limited to the Γ point. Again, the atomic positions were relaxed and the simulation were conducted with the optimized structure. The full optical absorption spectrum was calculated using a Liouville-Lanczos (LL) method to predict the polarizability ($\alpha(\omega)$). The LL method was employed within the Quantum Expresso TDDFT solver [22]. The range of frequencies (ω) was selected to be comparable to the experimental UV-VIS region. Details of the LL method are beyond the scope of this study but can be found in the literature [23]. The reader should be aware that the imaginary part the of the polarizability is related to the optical absorption and there was a user defined broadening term of 0.01Ry.

2 Experimental Details

A Zr-UiO-66-BDC-R family MOF materials were prepared following the procedure in the literature with modifications [10]. The same mole concentration for $ZrCl_4$ and organic linker BDC-R were dissolved in DMF, (1,4-benzenedicarboxylic acid for H, 2-amino-1,4-benzenedicarboxylic acid for NH_2 and 2-nitro-1,4-benzenedicarboxylic acid for NO_2, respectively). The resulting solution was transferred in Teflon-lined autoclave for 48 hours at 120°C. The precipitants were collected with centrifuge and washed with DMF and methanol, and then redispersed in methanol for three days with gentle stirring. After that, the solid was collected and dried at 120°C under vacuum. The UV-VIS absorption spectra for as-prepared MOF materials were measured on a Shimadzu 2550 UV-VIS spectrometer under the diffuse-reflection model using an integrating sphere (UV 2401/2, Shimadzu) coated with $BaSO_4$. FTIR and XRD data is provided in Section 6.

3 Results and Discussion

The discussion will begin with a study of the ground state prediction and their relative comparison. This will provide a quantitative comparison between the linker designs and the origins the modulations. Following this discussion will be a time-dependent density functional analysis that will compare the predicted UV-VIS spectrum to the experimentally obtained spectrum.

3.1 Density Functional Theory (DFT) Predictions

The ground state density functional theory (DFT) calculation were carried out on a optimized primitive unit cell. To aid in determining the role of the modifications to the linker design on the absorptive properties it was useful not only to investigate the total density of states (DOS) but also the projected density of states (PDOS). To further aid in the investigation the density of states, the states were projected back to the atomic orbital as shown in Figure 3 and the molecular orbitals as shown in Figure 4.

In Figure 3 all three of the linker designs are shown where each of the designs are grouped together by an arbitrarily shift along the y-axis. The band gap region for all the design is bound by the grayed region 1 and grayed region 3 in Figure 3. Within Figure 3 and Figure 4, an arbitrary displacement is imposed along the y-axis to aid in discussion between designs and orbitals. The top line in each design set is the total density of states and provides an collective perspective of the band gap for each design. The predicted band gap values for each of the designs are provided in the second column in Table 1. The band gap energy predicted in this study were commensurate with other studies [14]. The largest band gap for these linker designs is associated with the unmodified BDC linker, followed by the NO_2, and finally the NH_2. The DFT predictions are useful for a quantitative comparison between themselves, however, the absolute band gap energy is underestimated when compared to the experimental values, see last column of Table 1. This discrepancy of the band gap is a classic occurrence in DFT ground state predictions and arises from the approximations in the exchange-correlation.

In reference to the BDC-NO_2 linker design in Figure 3, there is a significant peak in the density of states between -3eV and -2.5eV (grayed region 2 in Figure 3) when compared to the original linker design (BDC). It is noted that this contribution of states is originated due to the donor states of p-orbitals as would be expected from the attached nitrogen atom that has a 2p valance state. Referring to the plot of projected molecular orbitals in Figure 4, it can be confirmed that both the carbon atoms and the nitrogen atoms are contributing to the state. It is reasoned that a hybridized sp2 bond between the carbon and nitrogen is present but with limited s-orbital content as noted by the negligible density of s-orbitals at that energy level. To further confirm the C-N interaction the integrated local density of states between -2eV and -1eV (grayed region 2) was plotted within the unit cell as depicted in Figure 5. Here the nitrogen atoms form complementary π-bonds with the carbon atoms in the aromatic ring. The DOS further indicate that the nitrogen forms s-orbital hydrogen type bonding with the outlying pair of hydrogen on the functional group resulting in a donor site. The distance between the H-N is 1.0192$\AA$ and the N-C is 1.3591$\AA$, which confirm this result of $H-N\cdots C$ hydrogen bonding between the H-N and the donor state of their bond. The H-N donor site contribute a valance state (grayed region 2) that can be seen in the DOS plots. This mid-gap donor state results in a decrease in the band gap of nearly 0.8eV when compared to the non-functionalized BDC linker.

The decrease in band gap energy of the BDC-NO_2 is less significant in magnitude when compared to BDC-NH_2 design because of the bonding nature between the functional group's nitrogen and the aromatic carbon. The prediction of the BDC-NO_2 linker design resulted in absolute band gap of 2.8eV. The slight decrease of 0.3eV when compared to non-functionalized BDC linker is realized by the addition of states near the valence band maximum (grayed region 1). From a ground state perspective there was not a large difference from the BDC case, as seen in Figure 3. However, experimental analysis reported a decrease in the band gap energy of approximately 0.83eV. This was reasoned to arise from the charge-transfer influences, which was not captured in the ground state calculation but were confirmed in the time-dependent calculation (see Section 2.2). However, the ground state calculation provides insight into the bonding nature through investigation of the partial density of states and the geometry of the functional group. It is noted in part c of Figure 2 that the angle of the NO_2 pendent attached to the aromatic ring is slightly rotated which was reasoned to arise from the directional nature of the sp2 hybridized bond between the functional group and the aromatic carbons. The functional group in this configuration is most likely an acceptor as the nature of the nitrogen-oxygen bond is not fully satisfied and accepts p-orbital electrons from the sp2 hybridized carbon atoms resulting in a slight modification of the p-orbitals as seen in Figure 3 when comparing BDC-NO_2 to BDC. This slight modification of the p-orbital and the acceptor nature of the functional group contribute a valance state near the valance band maximum modulating the band gap only slightly (0.3eV). In Figure 4 there is an obvious change in the contribution of states from the carbon atoms at the valence band maximum for BDC-NO_2 that is not present for BDC-NH_2. There is also a change in the oxygen states that is related to the oxygen on the NO_2 functional group. Therefore, the oxygen on the end of the functional group is interacting with aromatic carbons by rotating out of plane of the aromatic ring. In doing so the oxygen accepts electrons from the carbon atoms resulting in a shift of the carbon states at the valance maximum. A combination of nitrogen and oxygen interacting with the carbon results in the decrease of the band gap.

Linker Design	DFT	TDDFT	Experiment UV-VIS
BDC	3.10	3.78	3.76
BDC-NO_2	2.80	2.94	2.93
BDC-NH_2	2.20	2.79	2.75

Table 1 Calculated and experimentally determined band gap energies for three MOF linker designs. The DFT predictions were determined based on the ground state DOS band gap. The TDDFT prediction and the experimental results were determined from the UV-VIS spectrum shown in Figure 7. The experimental data was determined using a UV-VIS spectrometer.

A limiting aspect of organic semiconductor devices when compared to their inorganic equivalents is the diminished car-

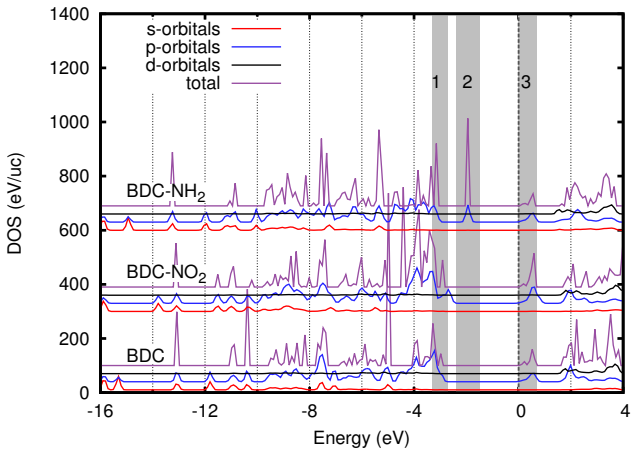

Fig. 3 Plot of the projected density of states of the atomic orbitals for the three MOF designs. The BDC-NH_2 has an effective ground state band gap of 2.2eV. The BDC-NH_2 design has a mid-gap valance state arising from the donor nature of the functional group. The DOS of each set of linker designs were offset in the y-dir for ease of comparison. The Fermi energy was also aligned for each of the designs.

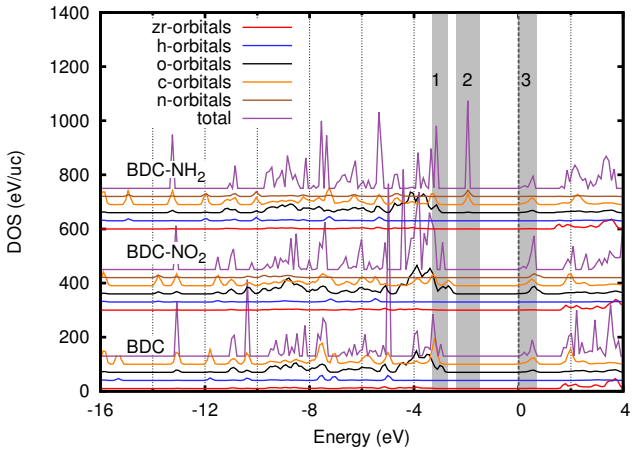

Fig. 4 Plot of the projected density of states of the molecular orbitals for the three MOF designs. The sp2 hybridized bonding state of the aromatic carbon and the nitrogen in the BDC-NH_2 are responsible for the mid-band gap state. A band gap of 2.2eV was realized BDC-NH_2 MOF. The DOS of each design was offset in the y-dir for ease of comparison.

rier mobility. To predict the mobility of the UiO-66 MOF the band structure was predicted from the ground state DFT calculation along the linker direction between k-points (1,0,0) and (0,1,1). It was assumed that the path of photoionized charge carriers is along the length of the linker. The band structure was determined from the single primitive unit cell, which included the metalloid corners. Often the bands in organics are

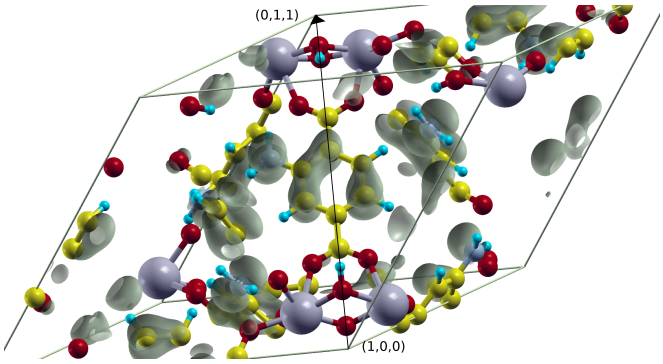

Fig. 5 Plot of the integrated density of state for the BDC-NH_2 design at an energy range between -2eV and -1eV that is associated with the grayed area (2) in Figure 3.

governed by a hopping mechanism, however, along this direction the bands were found to be smooth and on the same energy scale (not a large difference in energy of conduction band minima), therefore, a effective mass approach was implemented. For all of the linker designs, the Fermi level was closest to the conduction band minimum denoting a n-type conductivity. Thus, the mobility in this study will be limited to the lowest conduction band edge. However, the valance band maximum were noted to be flat indicating low hole mobility. This low hole mobility of the minority carriers will often be the limiting conduction mechanism. The reader should be aware that DFT is not appropriate to calculate the absolute conduction band edge but is used in a comparative manner in this study.

Assuming band like mobility of electrons in the lowest conduction band, a least squares fit of the band edge was calculated to determine the reduced effective mass. A plot of the band minima is shown in Figure 6 where the dashed lines highlight the effective mass fit. There were two minima in the band edge that were near the aromatic ring (0.5,0.5,0.5) and near the metal clusters. Both of these minima had identical effective mass of 8.9. This is reasoned to be a result of the sp2 bonding carbons atoms around the aromatic right and at the metal cluster. This can be confirmed from Figure 3 by the p-orbital contribution of the conduction band and in Figure 4 by the carbon contribution closest to the conduction band edge.

3.2 Time-Dependent Density Functional Theory (TDDFT) Predictions

As noted from the ground state calculation (see Section 2.1), there was a moderate underestimation of the band gap for all the linker design when compared to experimental UV-VIS results, see Table 1. It is well accepted that DFT predictions often underestimate the band gap but it is also reasoned that some additional discrepancy will arise when comparing to ex-

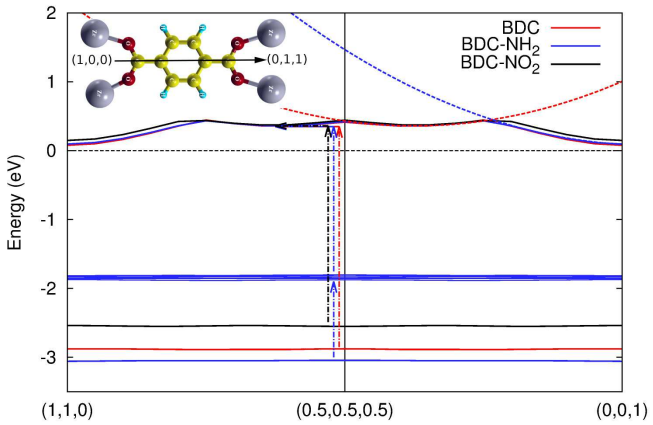

Fig. 6 Plot of the band structure along the vector (1,0,0) to (0,1,1), which corresponds to the length of the linker and is illustrated by vector in Figure 5. Only the valance maximum and conduction minimum are depicted. The dashed lines are a least square fit of the effective mass to the conduction band minimum. The dashed arrows illustrate the transition of electrons from the valance state to the conduction states.

perimental results because of the charge-transfer influences. Capturing the transient dipoles arising from a periodic perturbation are critical to actually predicting optical absorption in molecular structure. Therefore, a time-dependent density functional theory calculation was employed. To limit the computational expense of the TDDFT calculation, only the hydrogen terminated linkers were studied.

The predictions of the TDDFT calculation are shown in Figure 7 for all three linker designs. The corresponding band gap values are provided in Table 1. The TDDFT predictions of the band gap are in good agreement with experimental values. The TDDFT simulations slightly over-predicted the band gap when compared to experimental values. Most notable is the comparison of the TDDFT results of the BDC linker and experimental values. Because there was only a single linker simulated a user defined broadening term of 0.01Ry was associated with the line width of the TDDFT results. In both the BDC-NO_2 and BDC-NH_2 design there were two apparent peaks. The first peak at 250nm is associated with the sp2 bonds of the aromatic ring and is the sole peak in the BDC case. The second peak at 390nm for BDC-NO_2 and 410nm for BDC-NH_2 is associated with the functional group.

In providing an explanation of the time dependent response, the assumption was made that the functional group acts like a simple mass-spring system where the atomic masses of the functional group can be lumped together and the spring constant is related to the bonding between the functional group and the aromatic carbon. From molecular resonance point of view it is understood that when electromagnetic radiation is absorbed by the molecular structure an instantaneous dipole forms as an excited electrons moves from one region to another leaving a positive center. The dipole consist of a electron either transition from the aromatic carbon to the functional group in the case of NO_2 or from the functional group in the case of NH_2. This dipole across the aromatics and functional group can be related to a force applied to the simple spring mass system. If the frequency of the induced transient dipole is an integer of the dipole resonance frequency of the structure there will be strong absorption. This will be seen as a peak in the UV-VIS data in Figure 7.

As reasoned in Section 3.1, the modulation of the absorption stems from the bonding nature between the functional group and the aromatic carbon atoms. In the simple harmonic system analogy, the resonance frequencies are proportional the square root of the spring constant over the mass. Comparing NO_2 and NH_2 and assuming the mass is similar the relative bonding strength of the dipole can be approximated. The mass in this case is the mass of the electrons resulting in the dipole and not the atomic mass of the function group. From Figure 7 the ratio of optical absorption edges is approximately 5% between NO_2 and NH_2. Taking the ratio of ground state DFT prediction of the band gap is approximately 11%. The difference in these ratio is a result of charge-transfer between transition states. Therefore, the scattering cross-section and the scattering rate can be assumed to be approximately 11% larger for NH_2 compared to NO_2.

The ground state calculation the BDC-NO_2 linker was reasoned to have less band gap modulation because the acceptor nature of the O-C, which contributed states near the valence band maximum as a result of the oxygen interacting with the carbon. Opposed to the BDC-NH_2 case where mid-gap state was realized. In the time-dependent analysis the band gap is improved with predicted absolute band gap of 2.94eV for BDC-NO_2. However, a more significant change in the band gap was realized for the BDC-NH_2 linker where the donor-acceptor H-N bond influences the optical absorption response of the aromatic ring and the sp2 bonding the carbon and nitrogen. This finding provides evidence that the band gap can be further modulated if donor states from additional or improved functionalization can be localized near the sp2 carbon atoms or aromatic ring. It is suggested that large functionals groups even though they may have donor contributions may prove to be less significant if they are not localized around the aromatic carbon. This means that the functional group should focus on modifying the absorption properties of the sp2 carbon and less the functional group itself.

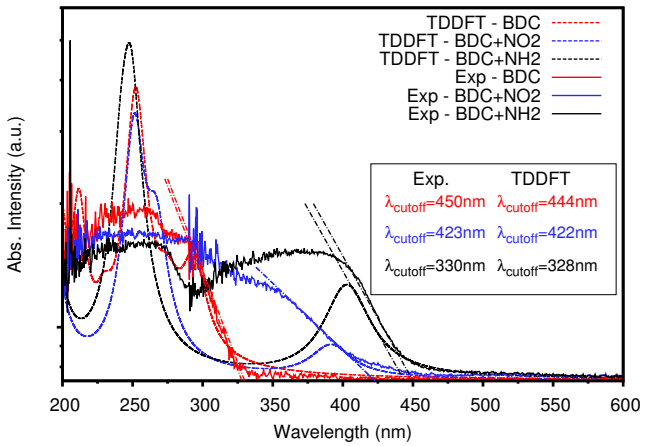

Fig. 7 Plot of the TDDFT predicted UV-VIS (dashed lines) and the experimentally determined UV-VIS (solid lines). The TDDFT predictions were based on only the linkers and the results were scaled so the peak intensity was on the order of the experimental data. The linear lines in the figure were used to extrapolate the cut-off wavelength to the x-intercept, which define the band gap energy.

4 Conclusion

A Zr-UiO-66 MOF structure with three linker design of BDC, BDC-NO_2, and BDC-NH_2 were investigated from a computational and experimental perspective. A ground state DFT calculation confirmed a decrease in the band gap energy, which was smallest for the BDC-NH_2 design. It was reasoned based on projected density of state predictions that the band gap modulation was a results of the p-orbital interactions of the functional group's nitrogen atom and the aromatic carbon atoms. A less significant modulation of the band gap was predicted from the ground state calculation of BDC-NO_2. This decreased modulation was reasoned based on the acceptor configuration of the functional group. A slight out of plane rotation of the BDC-NO_2 pendent indicated increased sp2 directional bonding between the nitrogen and carbon and additional interaction between the functional group's oxygen and carbon atoms. The electron effective mass of the all the linkers was estimated to be approximately $8.9m_e$. Time-dependent density functional calculations confirmed that the optical absorption peaks were result of the bonding nature of the sp2 carbon of the aromatic ring and the functional group. An 11% increase in the scattering cross-section was approximated for the NH_2 compared to NO_2. In conclusion, the band gap modulation was determined to be heavily influence by the bonding nature of the functional group with the aromatic carbon ring. This finding provides motivation for further study into new functionals that are not independently good optical absorbers but are able to influence the aromatic carbons role in optical absorption.

5 Acknowledgments

Acknowledgment is made to the Donors of the American Chemical Society Petroleum Research Fund (PRF# 53490-ND10) for partial support of this research.

6 Supplemental Material

Figure 8 a shows the FTIR spectra for MOF samples with different side groups. To clearly identify the groups in MOF, we also provided the FTIR spectra for organic precursors BDC, NO_2-BDC and NH_2-BDC in Figure 8b. The characteristics peaks for N-O stretching at $1357cm^{-1}$ and $1540cm^{-1}$ (Fig. 8c) can be observed in NO_2-UIO-66-Zr (Fig. 9a), and peaks for NH_2 vibrations at $3505cm^{-1}$ and $3394cm^{-1}$ (Fig. 9d) appear in NH_2-UIO-66-Zr (Fig. 8a). These observations agree well with the publication [24].

XRD pattern shows that the as-prepared UIO-66-Zr MOF powder is highly crystallized, which is in consistent with the reported literature [10]. The substitution with different side groups does not change MOFs crystalline structure.

References

1 H. Wu, Y. S. Chua, V. Krungleviciute, M. Tyagi, P. Chen, T. Yildirim and W. Zhou, *Journal of the American Chemical Society*, 2013, **135**, 10525–10532.
2 Q. Yang, A. D. Wiersum, P. L. Llewellyn, V. Guillerm, C. Serre and G. Maurin, *Chem. Commun.*, 2011, **47**, 9603–9605.
3 C.-K. Lin, D. Zhao, W.-Y. Gao, Z. Yang, J. Ye, T. Xu, Q. Ge, S. Ma and D.-J. Liu, *Inorganic Chemistry*, 2012, **51**, 9039–9044.
4 P. Canepa, N. Nijem, Y. J. Chabal and T. Thonhauser, *Phys. Rev. Lett.*, 2013, **110**, 026102.
5 K. Tan, P. Canepa, Q. Gong, J. Liu, D. H. Johnson, A. Dyevoich, P. K. Thallapally, T. Thonhauser, J. Li and Y. J. Chabal, *Chemistry of Materials*, 2013, **25**, 4653–4662.
6 J. Lee, O. K. Farha, J. Roberts, K. A. Scheidt, S. T. Nguyen and J. T. Hupp, *Chem. Soc. Rev.*, 2009, **38**, 1450–1459.
7 L. Hailian, E. Mohamed, M. O'Keeffe and O. M. Yaghi, *Nature*, 1999, **402**, 279.
8 C. H. Hendon, D. Tiana and A. Walsh, *Phys. Chem. Chem. Phys.*, 2012, **14**, 13120–13132.
9 J.-L. Wang, C. Wang and W. Lin, *ACS Catalysis*, 2012, **2**, 2630–2640.
10 J. Long, S. Wang, Z. Ding, S. Wang, Y. Zhou, L. Huang and X. Wang, *Chem. Commun.*, 2012, **48**, 11656–11658.
11 M. A. Nasalevich, M. G. Goesten, T. J. Savenije, F. Kapteijn and J. Gascon, *Chem. Commun.*, 2013, **49**, 10575–10577.
12 Y. Peng, V. Krungleviciute, I. Eryazici, J. T. Hupp, O. K. Farha and T. Yildirim, *Journal of the American Chemical Society*, 2013, **135**, 11887–11894.
13 Q. Yang and C. Zhong, *The Journal of Physical Chemistry B*, 2006, **110**, 655–658.
14 E. FlageLarsen, A. Ryset, J. H. Cavka and K. Thorshaug, *The Journal of Physical Chemistry C*, 2013, **117**, 20610–20616.
15 L. Valenzano, B. Civalleri, S. Chavan, S. Bordiga, M. H. Nilsen, S. Jakobsen, K. P. Lillerud and C. Lamberti, *Chemistry of Materials*, 2011, **23**, 1700–1718.

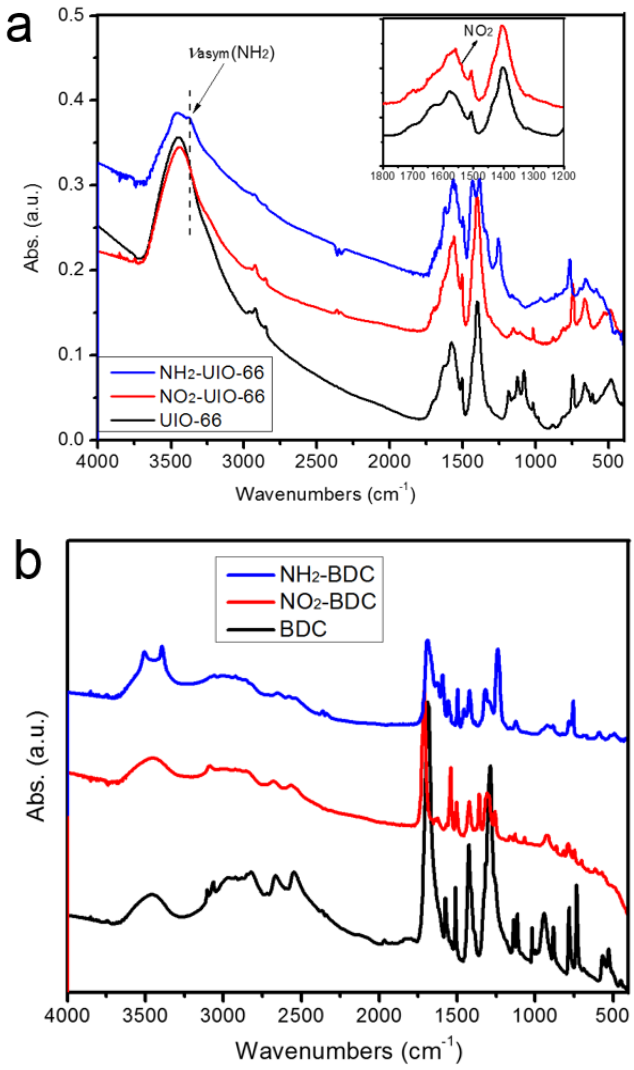

Fig. 8 FTIR spectra for MOF (a) and precursor organics (b) with different side groups.

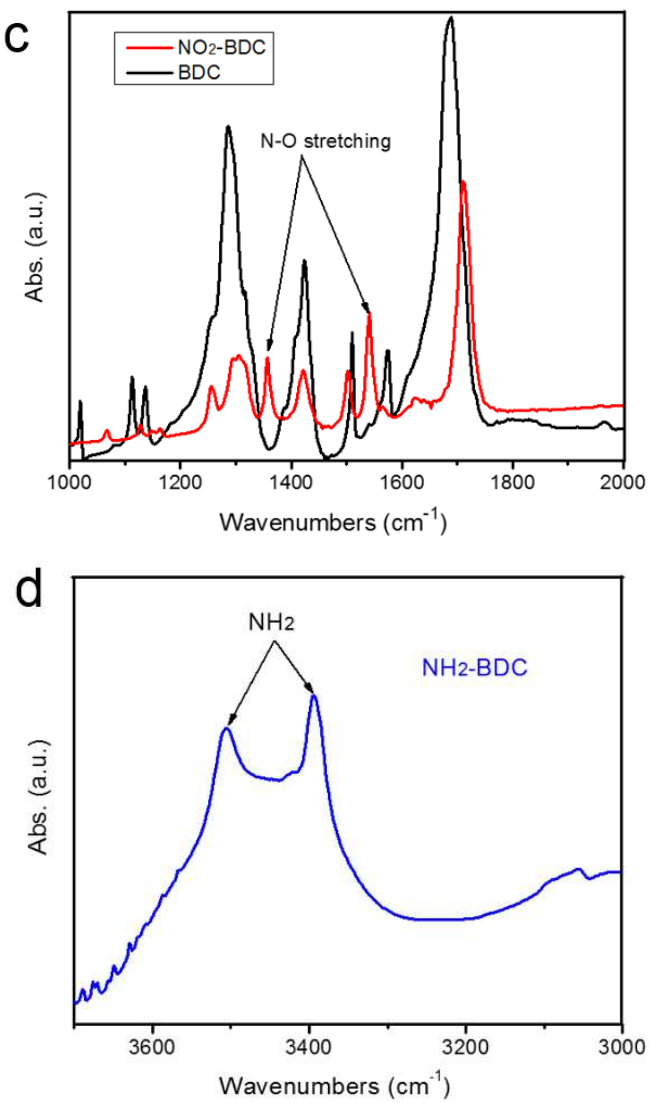

Fig. 9 FTIR spectra for MOF (c and d) are FTIR spectra with magnified wavenumber scale.

16 P. Giannozzi, S. Baroni, N. Bonini, M. Calandra, R. Car, C. Cavazzoni, D. Ceresoli, G. L. Chiarotti, M. Cococcioni, I. Dabo, A. D. Corso, S. de Gironcoli, S. Fabris, G. Fratesi, R. Gebauer, U. Gerstmann, C. Gougoussis, A. Kokalj, M. Lazzeri, L. Martin-Samos, N. Marzari, F. Mauri, R. Mazzarello, S. Paolini, A. Pasquarello, L. Paulatto, C. Sbraccia, S. Scandolo, G. Sclauzero, A. P. Seitsonen, A. Smogunov, P. Umari and R. M. Wentzcovitch, *Journal of Physics: Condensed Matter*, 2009, **21**, 395502.

17 W. Kohn, A. D. Becke and R. G. Parr, *The Journal of Physical Chemistry*, 1996, **100**, 12974–12980.

18 A. D. Becke, *The Journal of Chemical Physics*, 1993, **98**, 5648–5652.

19 B. Santra, A. Michaelides and M. Scheffler, *The Journal of Chemical Physics*, 2007, **127**,.

20 K. Sillar, A. Hofmann and J. Sauer, *Journal of the American Chemical Society*, 2009, **131**, 4143–4150.

21 T. Wang, Q. Zhang, B. Li, H. Chen and L. Chen, *International Journal of Hydrogen Energy*, 2012, **37**, 5081 – 5089.

22 D. Rocca, R. Gebauer, Y. Saad and S. Baroni, *The Journal of Chemical Physics*, 2008, **128**, –.

23 O. B. Malcolu, R. Gebauer, D. Rocca and S. Baroni, *Computer Physics Communications*, 2011, **182**, 1744 – 1754.

24 M. Kandiah, S. Usseglio, S. Svelle, U. Olsbye, K. P. Lillerud and M. Tilset, *J. Mater. Chem.*, 2010, **20**, 9848–9851.

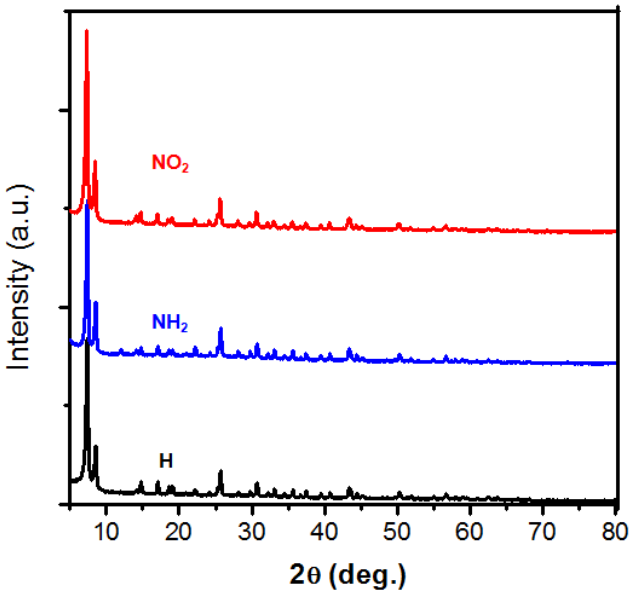

Fig. 10 XRD pattern for UIO-66-Zr with different side groups.